

Connecting Entropy Scaling and Density Scaling

Ian H. Bell,^{1, a)} Robin Fingerhut,² Jadran Vrabec,² and Lorenzo Costigliola³

¹⁾*Applied Chemicals and Materials Division, National Institute of Standards and Technology, Boulder, CO 80305*

²⁾*Technische Universität Berlin, Thermodynamics and Process Engineering, Ernst-Reuter-Platz 1, 10587 Berlin, Germany*

³⁾*Department of Science and Environment, Roskilde University, Postbox 260, DK-4000 Roskilde, Denmark*

(Dated: 1 June 2022)

It is shown that the residual entropy (entropy minus that of the ideal gas at the same temperature and density) is mostly synonymous with the independent variable of density scaling, identifying a direct link between these two approaches. The two-body residual entropy is demonstrated to not be a suitable surrogate for the total residual entropy in the gas phase. The residual entropy and the effective hardness of interaction (itself a derivative at constant residual entropy) are studied for the Lennard-Jones monomer and dimer as well as a range of rigid molecular models for carbon dioxide. It is observed that the density scaling exponent is related to the two-body interactions.

I. INTRODUCTION

Entropy scaling has been extensively studied in recent years (refer to Ref. 1 for a review) as a means of connecting dynamics and equilibrium thermodynamics. A requirement for applying this approach to the transport properties of real fluids is a reliable model for the residual entropy (the difference between the entropy and the entropy of an ideal gas at the same temperature and density), which is usually obtained from an empirical equation of state (EOS), or more computationally costly molecular simulation methods, limiting the usefulness of entropy scaling. Representing the residual entropy straightforwardly in terms of temperature and density would therefore be appealing and broaden the range of fluids for which entropy scaling might be applied. The goal of this work is to demonstrate that this representation is less impossible than it might seem, and furthermore, it reveals a heretofore unknown link between density scaling and entropy scaling approaches in the entire phase diagram.

As a first demonstration of the motivation of this paper, we overlay shear viscosity data of CO₂ as a function of the independent variable of each approach in Fig. 1. The dependent variable is $\eta^+ = \eta / (\rho_N^{2/3} \sqrt{mk_B T}) \times (s^+)^{2/3}$, where η is the shear viscosity, ρ_N is the number density, m is the mass of one entity (atom or molecule), k_B is Boltzmann's constant, T is the temperature and s^+ is the reduced residual entropy defined later on. The viscosity data were scaled according to the modified entropy scaling approach introduced in Ref. 2. The density scaling exponent of 13.5 was taken from Ref. 3. The quantity η^+ combines macroscopic scaling (a requirement for isomorph theory), and the plus-scaling introduced in Ref. 2. We will revisit each of the elements, but for now the key point is that the two approaches yield almost linear relationships in semi-log coordinates.

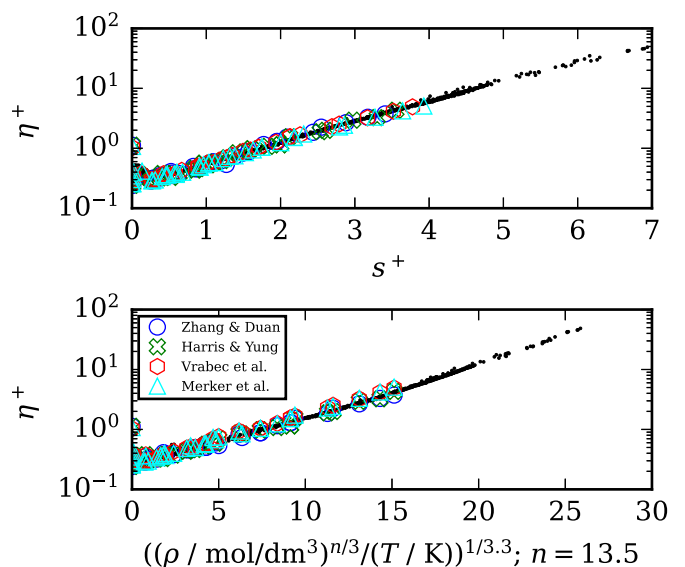


FIG. 1. Modified entropy scaling applied to shear viscosity data as a function of residual entropy (top panel) and density scaling variable (bottom panel) applied to shear viscosity data for CO₂ (open markers: selected simulation results from this work, points: experimental data collection from Ref. 2).

A. Entropy Scaling

The observation of a correlation between the variation of transport coefficients (e.g., self-diffusion coefficient or shear viscosity) of simple liquids and their residual entropy can be traced back to Rosenfeld in 1977⁴. In Rosenfeld's work, simulation results for different systems were presented and simple exponential relations between dimensionless values of self-diffusion coefficient or shear viscosity and residual entropy were proposed. A fundamental observation was that in order to observe these correlations between transport coefficients and residual entropy, the physical quantities need to be made dimensionless by using macroscopically reduced units⁵. In macroscopically reduced units, lengths are measured in terms

^{a)}Electronic mail: ian.bell@nist.gov

of the average interparticle distance $\rho_N^{-1/3}$, with ρ_N being the number density, and energies in terms of $k_B T$. A tilde above the quantity of interest will indicate in the following that the quantity is expressed in macroscopically reduced units. Similar results were later found by Dzugasov⁶ which was the start of a growing interest in the entropy scaling approach. While the initial focus was on understanding the nature of the relationship between residual entropy and scaled transport properties, this approach has been shown to be applicable to a broad range of fluids (as long as they behave classically and do not form strong directional bonds). The review of Dyre¹ in 2018 summarized the progress in this field up to that date. Since then, additional studies have considered the physical basis of this approach^{2,7}, and applied the technique to different systems: the Lennard-Jones fluid⁸, refrigerants^{9,10}, and alkanes^{11,12}.

B. Density Scaling

Density scaling is trivially valid for systems interacting via inverse-power-law (IPL) potentials of the form $V(r) \propto r^{-n}$, where r is the molecular center of mass separation. For this family of systems, the dynamic and thermodynamic properties are not functions of T and ρ independently but depend on their combination $\Gamma = T\rho^{-n/3}$. As a consequence, the thermodynamic surface of these systems is one-dimensional. IPL fluids exhibit a one-to-one mapping between Γ and residual entropy (see the supporting information of Ref. 2) and indeed, between Γ and all thermodynamic and transport properties with the application of an appropriate scaling.

The density scaling approach takes a fluid of interest governed by a non-IPL potential and expresses its macroscopically scaled transport properties in the form $\tilde{X} = f(T/\rho^{n/3})$, where X is one of shear viscosity, thermal conductivity, or self-diffusion coefficient, and n is in this case a fluid-specific constant for the entire phase diagram¹³. Density scaling is thus predicated on the assumption that the effective interaction potential between molecules can be approximated by $V \propto r^{-n}$. Density scaling has been investigated for a wide range of systems, including Lennard-Jones models, modified Buckingham fluids, metals¹⁴, flexible molecular analogs¹⁵, and has proven to be useful also in glass-forming liquids¹⁶. A major concern for using this approach is the evidence that the density scaling coefficient n has been shown to be not constant both in computer simulations¹⁷ and in experiments^{18,19}.

So, how can entropy scaling and density scaling be reconciled? This work demonstrates that the use of a constant exponent has the effect of making the unique variable of density scaling a monovariate function of residual entropy. In other words, density scaling with a constant effective hardness and entropy scaling are very close cousins.

C. Isomorph Theory

Both entropy scaling and density scaling indicate that a relation between the dynamics of fluids and their thermo-

dynamic properties exists (see for instance Fig. 1), but do not provide a satisfying explanation for *why* this is the case. Rosenfeld's reference to the hard sphere system in the dense fluid phase as an explanation for the success of entropy scaling is hard to accept in gas-like phases. The assumption that repulsion, modeled as IPL interactions, yields density scaling has been challenged, both with simulations and experiments. Simulations showed that $\tilde{X} = f(T/\rho^{n/3})$ is too simple an approximation¹⁷, and experiments^{18,19} indicate that, in general, the density scaling exponent depends on the thermodynamic state point. A way to consistently link density scaling and entropy scaling is provided by isomorph theory, briefly introduced below. For a more complete overview of the theory we refer to Refs. 1,20,21.

According to isomorph theory, it is possible to identify regions in the phase diagram of a given liquid in which its behavior is simpler. This region can be identified with simulations by evaluating where the correlation coefficient R_{Ros} ²² is greater than 0.9:

$$R_{\text{Ros}} = \frac{\langle \Delta U \Delta W \rangle}{\sqrt{\langle (\Delta U)^2 \rangle \langle (\Delta W)^2 \rangle}} \quad (1)$$

In the definition of R_{Ros} , ΔU and ΔW are the deviations of the instantaneous values of potential energy and virial from its average value, respectively. The $\langle \dots \rangle$ syntax indicates the average of the argument over a canonical ensemble. The quantity R_{Ros} can also be evaluated with experiments under some approximations, as in Fig. 3 of Ref. 23. In the $R_{\text{Ros}} > 0.9$ regions, the phase diagram of the system is effectively one dimensional and the structure and dynamics of the system are invariant, when expressed in the macroscopically reduced units introduced earlier, i.e., along curves of constant residual entropy, which are called isomorphs. These invariances have been verified in several works, both with computer simulations²⁴ and experiments²⁵.

In this way, isomorph theory provides a clear link between density scaling and entropy scaling, additionally predicting the invariance of reduced structure. The weak point of this approach is that its validity is limited to some regions of the phase diagram and cannot explain, for example, the validity of entropy scaling at low densities (i.e. below the critical density).

Isomorph theory also predicts that the density scaling exponent $n/3$ depends on the thermodynamic state, as confirmed by computer simulations and experiments. The density scaling exponent is the slope of the constant residual entropy curves and can be evaluated from simulations in the canonical ensemble using the fluctuation formula²¹:

$$n_{\text{eff}} = 3 \frac{\langle \Delta U \Delta W \rangle}{\langle (\Delta U)^2 \rangle} = 3 \left(\frac{\partial \ln(T)}{\partial \ln(\rho)} \right)_{s^r} \quad (2)$$

where ΔU and ΔW have the same meanings as in Eq. (1). This quantity can also be evaluated at any state point in experiments as shown in Ref. 18.

This work will explore the link between entropy scaling and density scaling in the entire phase diagram of several fluids, i.e. both in the region of the phase diagram where isomorph theory can explain this link and close to the gas-liquid

coexistence where this link is not clear. In order to clarify this issue, we consider three families of “simple” systems: the Lennard-Jones monomer, the Lennard-Jones dimer, and a range of molecular models for carbon dioxide. First we consider the residual entropy calculated for each system, we calculate its effective n , and finally, we show how the residual entropy and density scaling are connected.

II. METHODS

A. Thermodynamics

In order to lay out the thermodynamics, we start with the definitions of the relevant quantities. The residual entropy s^r is defined by

$$s^r \equiv s(T, \rho) - s^{(\text{ig})}(T, \rho) \quad (3)$$

where $s^{(\text{ig})}$ is the molar entropy of the ideal gas, and s is the total molar entropy. In practice, this difference is not evaluated directly, rather the residual Helmholtz energy and its derivatives are used to obtain the residual entropy s^r (e.g., see Eq. (6) of Ref. 2). Furthermore, it is conceptually useful to consider rather than s^r the non-dimensional term s^+ defined by

$$s^+ \equiv -s^r/R \quad (4)$$

where R is the molar gas constant. Other residual properties (residual pressure p^r , residual molar Helmholtz energy a^r , and residual isochoric molar heat capacity c_v^r) are defined analogously:

$$p^r \equiv p(T, \rho) - p^{(\text{ig})}(T, \rho) \quad (5)$$

$$a^r \equiv a(T, \rho) - a^{(\text{ig})}(T, \rho) \quad (6)$$

$$c_v^r \equiv c_v(T, \rho) - c_v^{(\text{ig})}(T) \quad (7)$$

The quantity $c_v^{(\text{ig})}$ has only temperature dependence, while the other ideal gas properties depend both on temperature and density.

The effective hardness n_{eff} is defined by²¹ (identical to Eq. (2))

$$n_{\text{eff}} \equiv 3 \left(\frac{\partial \ln(T)}{\partial \ln(\rho)} \right)_{s^r} = 3 \frac{\rho}{T} \left(\frac{\partial T}{\partial \rho} \right)_{s^r} \quad (8)$$

After some thermodynamic manipulations²⁶, the value of n_{eff} from Eq. (8) can also be written in the equivalent formulation

$$n_{\text{eff}} = -3 \frac{\rho \left(\frac{\partial s^+}{\partial \rho} \right)_T}{T \left(\frac{\partial s^+}{\partial T} \right)_\rho} = 3 \frac{\frac{1}{\rho} \left(\frac{\partial (p^r/R)}{\partial T} \right)_\rho}{c_v^r/R} \quad (9)$$

As will be shown later, the derivative $(\partial s^+/\partial \rho)_T$ is in general positive and $(\partial s^+/\partial T)_\rho$ is in general negative, and thus

n_{eff} should be positive for the molecular systems studied here. Other systems can yield negative values of n_{eff} ²⁷.

With the formalism of Lustig²⁸, the residual Helmholtz energy derivatives can be obtained simultaneously in one molecular simulation run. In that framework, the density scaling exponent is defined by

$$n_{\text{eff}} = -3 \frac{\Lambda_{01} - \Lambda_{11}}{\Lambda_{20}} \quad (10)$$

in which

$$\Lambda_{ij} = (1/T)^i (\rho)^j \left(\frac{\partial^i \partial^j (a^r/RT)}{\partial (1/T)^i \partial \rho^j} \right) \quad (11)$$

In the dilute-gas limit, where two-body interactions are fully captured by the second virial coefficient B_2 , n_{eff} is given by²⁹

$$\lim_{\rho \rightarrow 0} n_{\text{eff}} = -3 \frac{T \frac{dB_2}{dT} + B_2}{T^2 \frac{d^2 B_2}{dT^2} + 2T \frac{dB_2}{dT}} \quad (12)$$

which has recently been derived in terms of the pair potential for an infinite number of spatial dimensions³⁰, where the infinite spatial dimension limit is equivalent to the two-body limit in Eq. (12).

B. Simulation Details

The Lennard-Jones monomer was simulated using the RUMD software package³¹. The potential was cut and shifted at the distance of 2.5σ and the potential parameters of σ and ϵ/k_B were set to unity. The temperature was controlled with a Nosé-Hoover thermostat using $\tau = 0.2$ as relaxation time. The timestep for the simulation was kept constant in macroscopic reduced units $d\tilde{t} = 0.001$ and the system size was $N = 1000$. The values of n_{eff} were obtained from the fluctuation formula in Eq. (2). The dependence of n_{eff} on the system size has been studied in appendix B of Ref. 30.

For the other fluids, molecular dynamics (MD) simulations were performed solving numerically Newton’s equations of motion with a fifth-order Gear predictor-corrector scheme by using the molecular simulation tool *ms2*^{32–35}. All simulations were sampled in the canonical ensemble with the formalism of Lustig²⁸ to calculate the Helmholtz energy derivatives with respect to density, inverse temperature as well as their combinations. Velocities were isokinetically rescaled to maintain the specified temperature. All CO₂ models given in Table I were simulated with *ms2* as well as the Lennard-Jones (LJ) dimer, which was set to a fixed bond length of σ . The long-range interactions were corrected with the usual analytic mean-field equations^{32–35}. Radial distribution functions were sampled over the entire simulation run to calculate the two-body residual entropy, results of which are shown in the supplementary material. Chemical potential data μ_i were determined with Widom’s test particle insertion method³⁶. The shear viscosity was obtained by applying the Green-Kubo formalism^{37,38} and

the Einstein relations³⁵ for the LJ dimer and the selected CO₂ models of Zhang and Duan, Harris and Yung, Vrabec, Stoll, and Hasse, Merker *et al.*, Errington and Hellmann.

The LJ dimer was studied in the temperature range $k_B T/\epsilon = 0.9$ to 100 and density range $\rho\sigma^3 = 0.00017$ to 0.5 with $N = 1372$ particles, whereas for transport properties $N = 4000$ were used. For that purpose, simulations were equilibrated by 100 Monte Carlo (MC) cycles and 10^5 MD time steps. The production runs were performed for a period of $4 \cdot 10^6$ (transport: $3 - 5 \cdot 10^7$) time steps with $\Delta t/(\sigma\sqrt{m/\epsilon}) = 0.0005$ (respectively 0.001 near the vapor-liquid equilibrium region). Intermolecular interactions were explicitly calculated up to the cutoff radius $r_c = 4\sigma$.

Each CO₂ model listed in Table I was evaluated in the temperature range $T = 250$ to 10,000 K and density range $\rho = 0.1$ to 25 mol/dm³ with $N = 1372$ molecules and a cutoff radius of $r_c = 14$ Å (transport: $N = 4000$, $r_c = 17.5$ Å). 200 MC cycles and $5 \cdot 10^5$ MD time steps were used for equilibration and the production was performed for a period of $4 \cdot 10^6$ (for transport at least $15 \cdot 10^6$) time steps with $\Delta t = 0.971$ fs (for $T = 250$ to 600 K: $\Delta t = 1.942$ fs). Besides that, some phase space regions of the Hellmann CO₂ fluid had to be simulated with different settings. At $T = 10,000$ K from $\rho = 9$ to 25 mol/dm³, an equilibration of 200 MC cycles and $8 \cdot 10^5$ MD time steps was performed followed by a production of $8 \cdot 10^6$ time steps with $\Delta t = 0.104$ fs.

The use of the formalism of Lustig²⁸ to calculate all thermodynamic properties from the same simulation run yields the n_{eff} values directly from its definition in Eq. (10)⁴⁵. The molecular models considered for CO₂ are listed in Table I.

The first four CO₂ models are qualitatively similar; they consist of three Lennard-Jones sites and point charges at each site. The next three models use two or three Lennard-Jones sites, along with a point quadrupole at the center of the molecule. The exception to this general approach are the models of Hellmann⁴⁴ and Errington^{43,49}. In these more advanced models, repulsion is roughly exponential in its form, and in the case of Hellmann⁴⁴, empirical potentials have been fitted to each site-site interaction term, in order to match first principles calculations of the potential energy surface.

The quadrupole moment of CO₂ is equal to $(-14.31 \pm 0.74) \times 10^{-40}$ C m², according to recent measurements of Chetty and Couling⁵⁰, which is consistent with other recent analysis⁵¹. The quadrupole moment of the molecular models are given in Table I. There is not a very strong correlation between the quadrupole moment Q and the representation of the data considered in this work. The details of the evaluation of each potential are covered in the source code of *potter*⁵². All calculations were done in SI units to ensure dimensional consistency.

Very precise second virial coefficients, their temperature derivatives, and values of n_{eff} of these models were calculated with the approach described in Ref. 29, with the use of the open-source *potter* library and multicomplex algebra to obtain B_2 and its temperature derivatives simultaneously. The integrator was allowed to evaluate the integrand as many as 10^7 times for each temperature.

III. RESIDUAL ENTROPY

The residual entropy is the independent variable of the macroscopically scaled transport properties in the entropy scaling framework and quantifies the loss of microstates of the system from intermolecular interactions. Residual entropy is a property that is not accessible experimentally, so it remains somewhat clouded in mystery. A comprehensive study of the residual entropy obtained from empirical thermodynamic models is called for.

A. All-Body s^+

For the Lennard-Jones fluid, values of s^+ can be obtained by thermodynamic integration⁵³ or other sampling-based methods, and the EOS of Thol *et al.*⁵⁴ gives a faithful representation of this quantity. Figure 2 presents the values of s^+ as a function of temperature and density for the Lennard-Jones fluid.

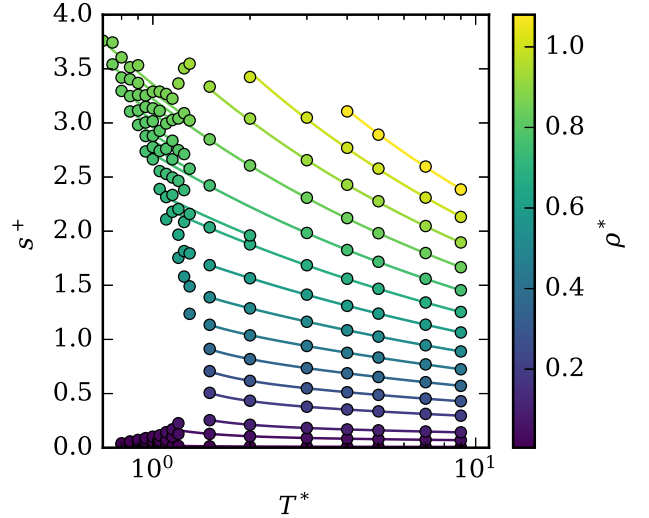


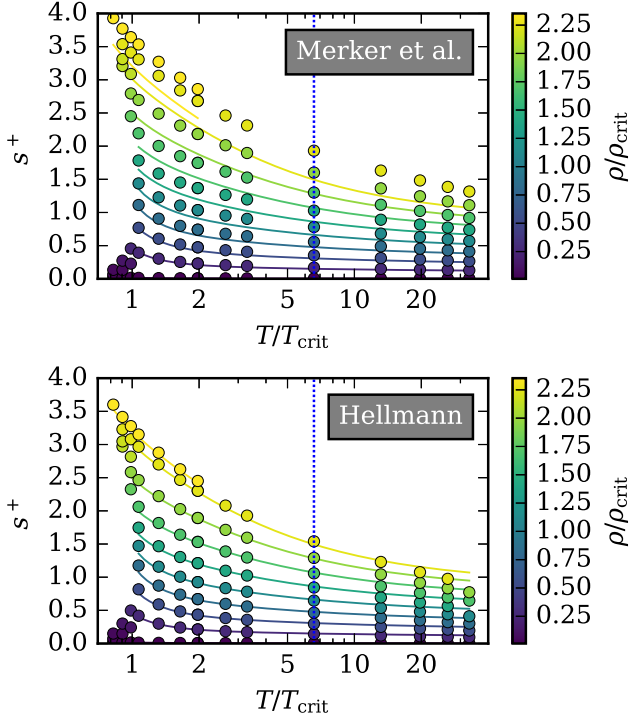
FIG. 2. Values of s^+ for the Lennard-Jones fluid. Markers are corrected simulation results from Ref. 54 and curves are from the EOS of Thol *et al.*⁵⁴

In this work, we compare the values of s^+ obtained for the thermodynamic models for CO₂ with each other and with the empirical EOS of Span and Wagner⁵⁵. Figure 3 shows the residual entropy calculated with two molecular models, those of Hellmann and Merker *et al.*, with the results from the Span and Wagner EOS overlaid. This result shows that the Hellmann molecular model provides a much closer agreement with the values of s^+ obtained from the EOS of Span and Wagner than the molecular model of Merker *et al.* For $T/T_{\text{crit}} \lesssim 20$, it is difficult to distinguish the markers (from the molecular model of Hellmann) and the curve (from Span and Wagner). To make the comparison more quantitative, Fig. 4 shows the deviations between the simulation data and the EOS. The other molecular models generally yield similar

TABLE I. Molecular models for CO₂ considered in this work.

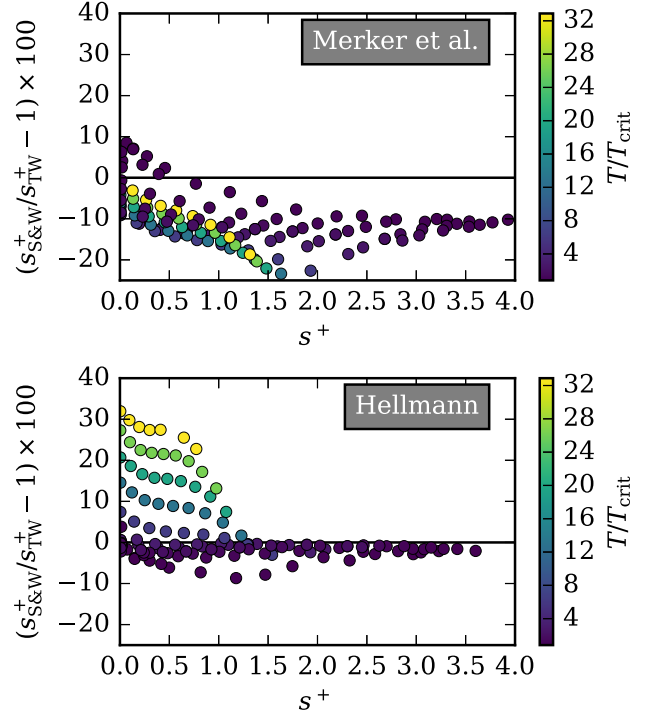
Author	N_{sites}	site-site	quadrupole	$Q \times 10^{40} / \text{C m}^2$
Murthy et al. ⁴⁶	3	LJ	point charges	-12.6
Potoff & Siepmann ⁴⁷	3	LJ	point charges	-15.1
Zhang & Duan ³⁹	3	LJ	point charges	-12.8
Harris & Yung ^{a40}	3	LJ	point charges	-13.7
Möller & Fischer ⁴⁸	2	LJ	point quadrupole	-12.2
Vrabec et al. ⁴¹	2	LJ	point quadrupole	-12.7
Merker et al. ⁴²	3	LJ	point quadrupole	-13.6
Errington ^{43,49}	3	EXP-6	point charges	-13.5
Hellmann ⁴⁴	7	empirical	point charges	-14.2

a: PM2, rigid

FIG. 3. Results for s^+ from the CO₂ molecular models of Merker *et al.*⁴² and Hellmann⁴⁴. The curve for each isochoire is given by the Span and Wagner EOS⁵⁵. The vertical dashed line indicates the temperature limit of the EOS at 2000 K.

results to that of Merker *et al.*, showing large deviations in residual entropy relative to the EOS. For the Hellmann model, for temperatures below the limit of the EOS at 2000 K⁵⁶, the mean absolute relative percentage error (MAPE) in s^+ is 2.1%. One distinguishing feature of the Hellmann model is its representation of the effective hardness n_{eff} , as shown in Section V. The differences are already evident at the level of classical calculations based upon the second virial coefficient.

For a state point either above the critical temperature, or in the gaseous phase for subcritical temperatures, scaled residual entropy at a given state point can be obtained by an integral

FIG. 4. Deviations of s^+ calculated from the CO₂ molecular models of Merker *et al.*⁴² and Hellmann⁴⁴ (subscript TW) from the Span and Wagner EOS⁵⁵ (subscript S&W).

taken at constant temperature

$$s^+ = \int_0^p \left(\frac{\partial s^+}{\partial \rho} \right)_T d\rho \quad (13)$$

where s^+ in the zero density limit (that of the ideal gas) is zero. This is the typical “thermodynamic integration” approach familiar to molecular simulation practitioners, formulated in a different fashion. An alternative (and thermodynamically identical) representation of Eq. (13) is

$$s^+ = \int_0^p \frac{1}{\rho^2} \left(\frac{\partial (p^r/R)}{\partial T} \right)_\rho d\rho \quad (14)$$

The formulation in Eq. (14) highlights the importance of high

quality densimetry data (measurements of density ρ as a function of temperature and pressure) for the representation of residual entropy. If the temperature and density dependence of pressure is well captured by laboratory measurements, the derivative $(\partial p^r/\partial T)_\rho$ will also be, and the residual entropy obtained from a highly accurate empirical model fitted to these data will also be accurate. In the case of CO₂ therefore, we may reasonably assume that the residual entropy obtained from the Span and Wagner EOS is probably correct within its range of validity given the large quantity of high quality densimetry data, and the excellent agreement of this EOS with these data⁵⁵.

At low density, s^+ is governed by the leading term of the virial expansion as explained in Section 3 in the supporting information:

$$\lim_{\rho \rightarrow 0} s^+ = \left(B_2 + T \frac{dB_2}{dT} \right) \rho_N \quad (15)$$

so the behavior of $\Theta_2 = B_2 + T(dB_2/dT)$ can provide information on the quality of the molecular model and that of the EOS. Figure 5 shows the obtained values of $B_2 + T(dB_2/dT)$ for each model and the EOS. The model values were obtained classically with *potter*. The quantity Θ_2 must be positive for all temperatures because the entropy must be less than that of an ideal gas at the same temperature and density, a constraint fulfilled by all molecular models and the EOS, but the qualitative behavior of the EOS is incorrect (compared with the Hellmann model) above approximately 1000 K. The reproduction of dilute gas residual entropy values in the low-density gas (considering values of Θ_2) is thus shown to be a sensitive test for the residual entropy.

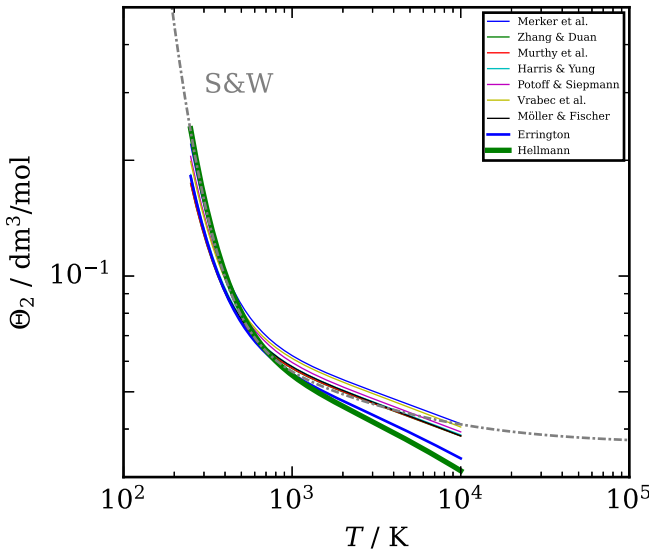


FIG. 5. Values of $\Theta_2 = B_2 + T(dB_2/dT)$ from molecular models and from the Span and Wagner⁵⁵ (S&W) EOS for CO₂.

B. Two-Body s_2^+

The all-body residual entropy is an inconvenient quantity to access when desiring to apply entropy scaling. In simulations, insertion methods⁵⁷ or thermodynamic integration⁵³ are required to obtain the residual entropy. In the real world, an equation of state is required, which is not always available for many classes of fluids. A convenient estimation of the total s^+ is to consider just the two-body part, a quantity that is accessible from the radial distribution function and can be straightforwardly obtained in simulation.

The total excess entropy can be given as the summation⁵⁸

$$s^+ = \sum_{n=2}^{\infty} s_n^+. \quad (16)$$

It is commonly assumed in the entropy scaling literature that the two-body residual entropy s_2^+ is a sufficiently good representation of the total s^+ (Ref. 58). Where isomorph theory is valid (especially in the liquid phase), the same scaling that applies for s^+ should necessarily apply for s_2^+ (Refs. 21,27). In the gas phase, entropy scaling still works well, although by rights it should not. *So, it is sufficient to use the s_2^+ in place of s^+ in general?*

As a test we have calculated the two-body residual entropy for each of the models for CO₂. To do so, the radial distribution function (RDF) g_{ij} data for each atom pair was obtained for all CO₂ molecular models, and then integrated to obtain the $s_2^+ \equiv -s_2/k_B$ via

$$s_2^+ = 2\pi\rho_{\text{atom}} \sum_{ij} x_i x_j \int_0^{\infty} (g_{ij}(r) \ln(g_{ij}(r)) - g_{ij}(r) + 1) r^2 dr \quad (17)$$

where x_i is the mole fraction of the atom, with i or j being either C or O. A subtle but important point about the two-body residual entropy of molecular systems is that ρ_{atom} is the number density of *atoms* (so atoms per volume), not the number density of sites or molecules. For molecular models where the number of sites matches the number of atoms (CO₂ has three atoms), the distinction is moot, but some CO₂ models have a number of sites that does not match the number of atoms: Möller & Fischer⁴⁸ (two sites), Vrabec et al.⁴¹ (two sites), Hellmann⁴⁴ (seven sites). This site/atom mismatch causes the two-body residual entropy to yield significantly different values.

Another mysterious feature of the two-body s_2^+ is that its dilute-gas limit does *not* match that of the total s^+ in general. Mathematically,

$$\lim_{\rho \rightarrow 0} s_2^+ \neq \left(B_2 + T \frac{dB_2}{dT} \right) \rho_N \quad (18)$$

This result is perplexing because s_2 is about two-body effects, and so is the second virial coefficient. Therefore, it stands to reason that the dilute-gas limit of s_2^+ should converge to that of s^+ , but that is not the case. Values of s_2^+ in the gas phase were obtained in this study, and the derivative

$$\Theta_{2,s_2^+} = \frac{s_2^+(\rho_{\min}) - 0}{\rho_{\min} - 0} \quad (19)$$

is the effective two-body version of Θ_2 obtained by finite differentiation, where ρ_{\min} is the lowest density at which the calculation was carried out. The values are plotted in Fig. 6, from which it appears that the infinite temperature limit is the same as Θ_2 for the total s^+ .

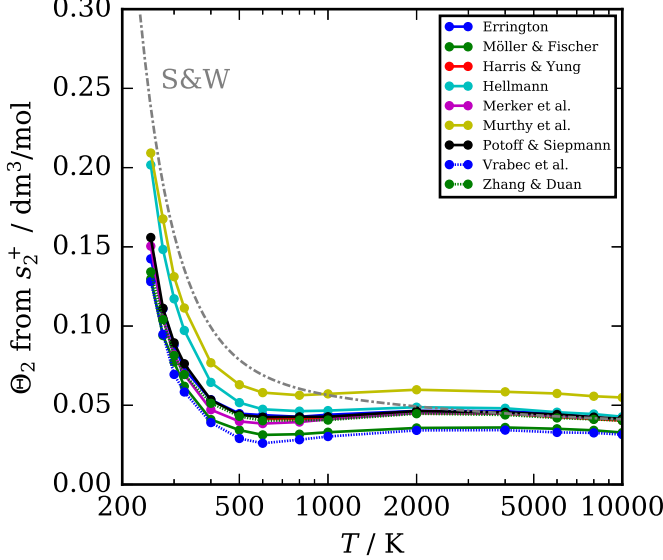


FIG. 6. Values of Θ_2 obtained from calculations of s_2^+ as a function of temperature.

IV. DENSITY SCALING AND ENTROPY SCALING

To begin our comparison between density and entropy scaling, we follow the approach taken in density scaling: the use of a constant n for the entire phase diagram in the definition of Γ . In the case of the Lennard-Jones monomer fluid, there is a particular value of n which maximizes the correlation between $(\rho^*)^{n/3}/T^*$ and s^+ . With this optimized value, the Spearman correlation coefficient between $(\rho^*)^{n/3}/T^*$ and s^+ is greater than 0.999, which represents nearly one-to-one relationship. The MD data also consider the gaseous phase and the critical region so that most of the phase diagram is covered. In order to assist with the visualization, the value of Γ^{-1} was scaled with an exponent to linearize the relationship between Γ^{-1} and s^+ in Fig. 7. This figure demonstrates that in the case of the Lennard-Jones monomer, s^+ and Γ^{-1} are directly connected to each other. The particular surprise in this figure is that the relation between Γ and s^+ holds even in parts of the phase diagram where $R_{\text{Ros}} \ll 0.9$. In the dilute-gas limit, this scaling should break down because the leading term from the virial expansion is defined as in Eq. (15) which does not follow the same scaling.

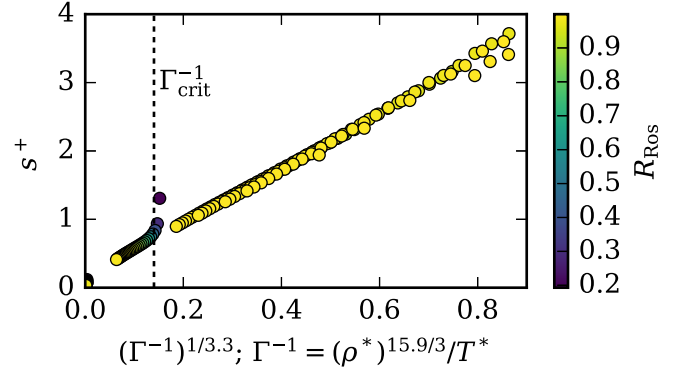


FIG. 7. Scaled values of s^+ for the Lennard-Jones monomer compared with density scaling values for $T^* < 20$.

For the Lennard-Jones dimer, the qualitative picture is similar, as shown in Fig. 8. Again, a constant value of n was selected that maximized the Spearman correlation between $(\rho_s^*/2)^{n/3}/T^*$ and s^+ . The addition of the bond to form a linear molecule does not appear to alter the core conclusion that a fixed value of n is needed to form a one-to-one relationship between $(\rho^*)^{n/3}/T^*$ and s^+ . For some of the state points with $R_{\text{Ros}} < 0.3$, indicating a breakdown of isomorph theory, the mapping between the variables is slightly less strong, but aside from these deviating points, the mapping is nearly as one-to-one as for the Lennard-Jones monomer. The values of s^+ for the dimer are approximately two times larger than those of the monomer at the same monomer density and temperature (microstates are removed by the fixed bond, limiting the accessible phase space). The state point dependence is shown in Fig. S1 in the supporting information.

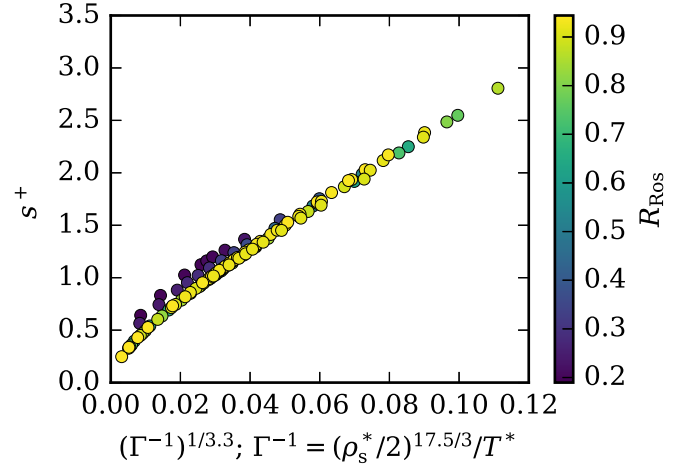


FIG. 8. Values of s^+ for the Lennard-Jones dimer from the present simulations compared with density scaling values. Note that the density ρ_s^* is the reduced monomer number density.

For the CO_2 model of Hellmann⁴⁴, the behavior is much the same as for the Lennard-Jones dimer. Again, n was selected to maximize the Spearman correlation between $\rho^{n/3}/T$ and s^+ for the points with $R_{\text{Ros}} > 0.5$. Figure 9 shows the same

type of plot, but with one striking difference. The relationship between s^+ and $(\Gamma^{-1})^{1/3.3}$ is qualitatively different. The curvature is convex in the case of CO_2 and concave in the case of the Lennard-Jones monomer and dimer.

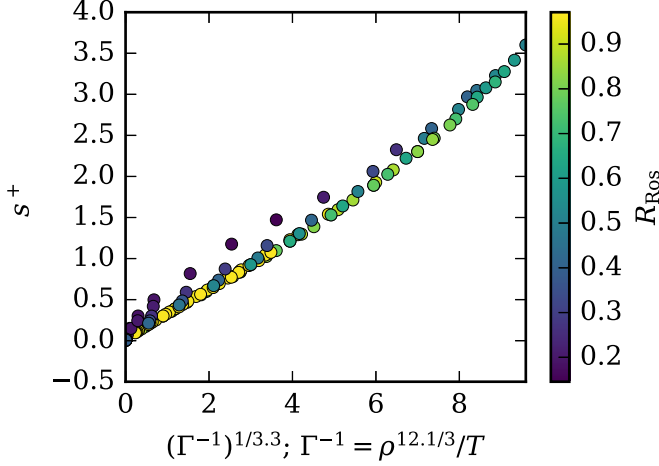


FIG. 9. Values of s^+ from the Hellmann⁴⁴ model for CO_2 from the present simulations as a function of the density scaling values. Density ρ is in units of mol/dm^3 and temperature T is in units of K.

V. EFFECTIVE HARDNESS

The analysis above primarily focused on *post hoc* analysis of simulation data in order to determine the optimal value of n for a particular system. *What if the optimal value of n is unknown?* A first glimpse of a predictive model for the optimal n comes from a consideration of the effective hardness of interaction n_{eff} . The quantity n_{eff} entered the vocabulary of thermodynamics with the advent of isomorph theory. The effective hardness can be conceptually thought of as the effective repulsiveness of the interactions between molecules⁵⁹. This intuitive understanding is somewhat incomplete, but gives a flavor.

A. Lennard-Jones monomer

We first consider the density scaling exponent n_{eff} obtained from MD simulations for the Lennard-Jones fluid. The results of these simulations are shown in Fig. 10. The calculations extend from the dilute gas up to extremely high temperatures and very dense liquid states. The dilute-gas values obtained from the second virial coefficient²⁹ are also shown, highlighting that the values approach 12 in the infinite temperature limit. In this high-temperature limit, the interactions are entirely governed by the repulsive contribution (which is proportional to r^{-12} for the Lennard-Jones fluid). For densities and temperatures more aligned with engineering applications, n_{eff} has both temperature and density dependence. Along the critical isotherm, the values of n_{eff} vary from approximately 16 to zero (going towards zero at the critical point); n_{eff} is de-

cidedly not constant for even simple systems like the Lennard-Jones fluid.

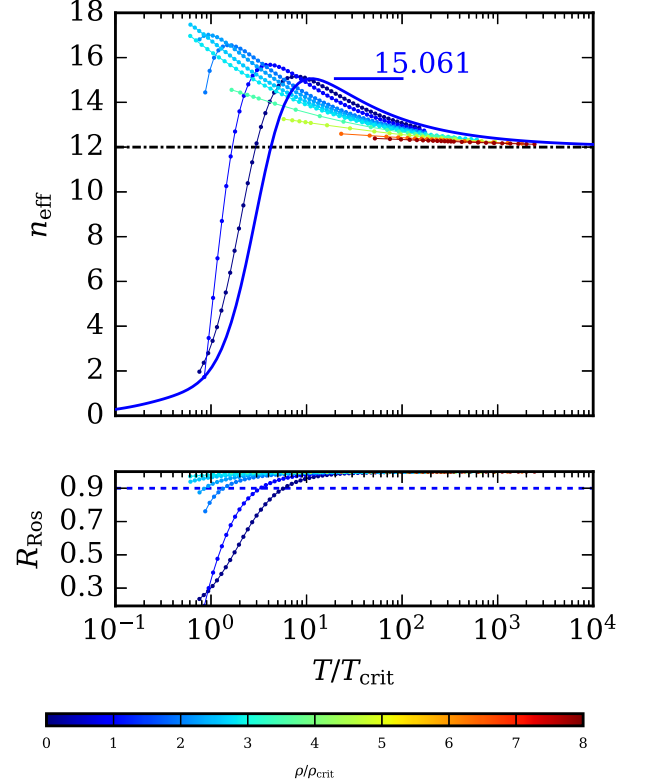


FIG. 10. Values of n_{eff} and R_{Ros} for the Lennard-Jones monomer fluid. The thick curve is the value obtained from the closed form solution for the second virial coefficient published by Sadus^{60,61}, and other values were calculated from NVT simulations performed with the RUMD software package³¹.

The integration from Eq. (13) may equivalently be written in terms of n_{eff} as

$$s^+ = \frac{1}{3} \int_0^\rho \frac{(c_v^r/R)n_{\text{eff}}}{\rho} d\rho \quad (20)$$

This expression provides a useful way of thinking about the relationship between residual entropy and n_{eff} . The conceptual lesson of Eq. (20) is that if n_{eff} and c_v^r obtained from an EOS or molecular model are both correct, the residual entropy will also be. Conversely, if the values of s^+ are thought to be correct, and the n_{eff} is correct, the isochoric heat capacity should also be correct. However, experimental measurements of heat capacities for fluids are often characterized by relatively large experimental uncertainties, inconsistency, and in many cases by a complete lack in the open literature.

At temperatures well above the critical temperature, n_{eff} depends only relatively weakly on density³⁰ and the representation of the residual entropy is therefore largely governed by the dilute-gas n_{eff} . For instance in Fig. 10, for $T > 10T_{\text{crit}}$ the variation of n_{eff} is within roughly 30% of the infinite temperature limit of 12. This is why density scaling with a constant n

works reasonably well when studying a narrow region in the liquid region of the phase diagram, but not otherwise. Following Eq. (20), constraining or obtaining the correct dilute-gas value for n_{eff} also constrains much of the liquid phase residual entropy. For liquid states, most of the variation in n_{eff} for the Lennard-Jones monomer corresponds to the region close to the critical point.

B. Lennard-Jones dimer

Ref. 29 considered the n_{eff} in the dilute-gas limit for rigid linear chains with Lennard-Jones sites. The values of n_{eff} in this work were obtained with a similar method (integration with *potter* over three angles and center-of-mass separation), and are shown in Fig. 11. The fundamental difference between the Lennard-Jones monomer and dimer is only one of magnitude; the qualitative behavior is similar, and the vertical axis is mostly just scaled. In the infinite-temperature limit, the value of n_{eff} also approaches 12 because at sufficiently high temperatures the dominant interaction is the pairwise repulsion of two sites governed by an r^{-12} interaction²⁹.

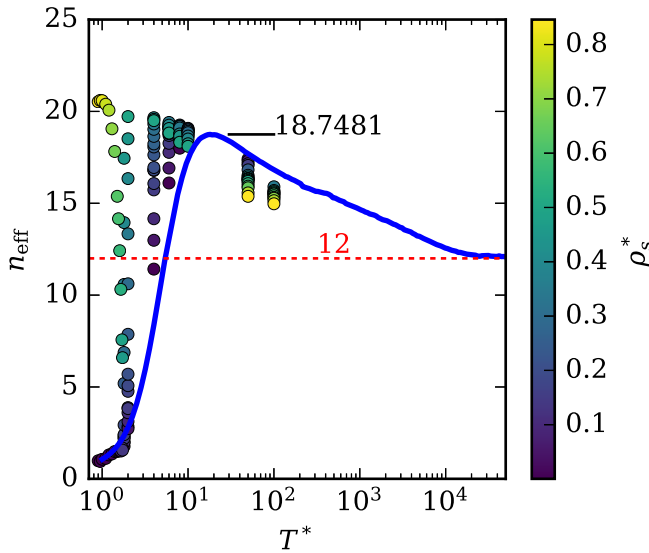


FIG. 11. Values of n_{eff} for the Lennard-Jones dimer fluid as a function of temperature and monomer density ρ_s^* (which is twice the reduced molecular density). The dilute-gas limit (solid curve) was taken from Ref. 29 and the markers are the simulation data from this work.

C. Carbon dioxide

The molecular models used in this work for CO_2 are linear and rigid and do not allow for vibrational contributions to the energy. The dilute-gas limit of n_{eff} can therefore be obtained, as described above, from four-fold integration. Classical values of n_{eff} are shown in Fig. 12 for the considered molecular models as a function of temperature. The *ab ini-*

tio potential of Hellmann⁴⁴ can yield very accurate predictions of the dilute-gas thermophysical properties (e.g., second virial coefficient). As such, and especially given the physically sound basis of this model, it is believed that the values of n_{eff} from the Hellmann⁴⁴ model in the dilute-gas limit are therefore a suitable baseline for a comparison with other models. The values of n_{eff} calculated from the model of Hellmann are smaller than those of the other models at all temperatures. The model of Errington (which has a more physically sound exponential repulsion as compared with the r^{-12} repulsion of the other models), is much closer than the other models, which are mostly consistent, but with larger values. The value of n for CO_2 proposed in the literature for density scaling³ is 13.5 based upon density scaling of shear viscosity data in the liquid phase, which is near the peak value of 13.24 obtained for n_{eff} from the Hellmann⁴⁴ model.

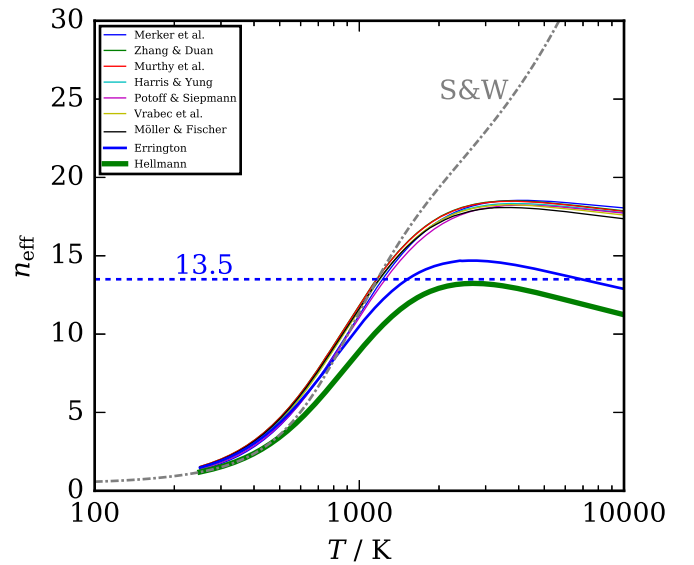


FIG. 12. Values of n_{eff} in the dilute-gas limit (from Eq. (12)) obtained by *potter* for the CO_2 molecular models and from the Span and Wagner⁵⁵ (S&W) EOS.

Next, the values of n_{eff} from the molecular models are plotted as a function of temperature and density. Given the qualitative similarities, only the results for the Merker et al. and Hellmann potentials are shown here; the remainder are in the supporting information. Many qualitative features of these results are similar to those of the Lennard-Jones fluid. At high temperatures ($T/T_{\text{crit}} \gtrsim 20$), n_{eff} does not change much as the density is swept through a large range, and the temperature at the maximum of n_{eff} along an isochore does not depend strongly on the density; it is close to the maximum obtained from the dilute-gas calculations. The infinite temperature limit for CO_2 (unphysically neglecting dissociation) should be 3/2 (see the appendix of Ref. 62), which holds for all potentials that are finitely valued at all separations. For the Hellmann model, the contributions to the potentials are divergent at a center-of-mass separation of zero, and a small hard core is required for each site-site interaction, which makes the

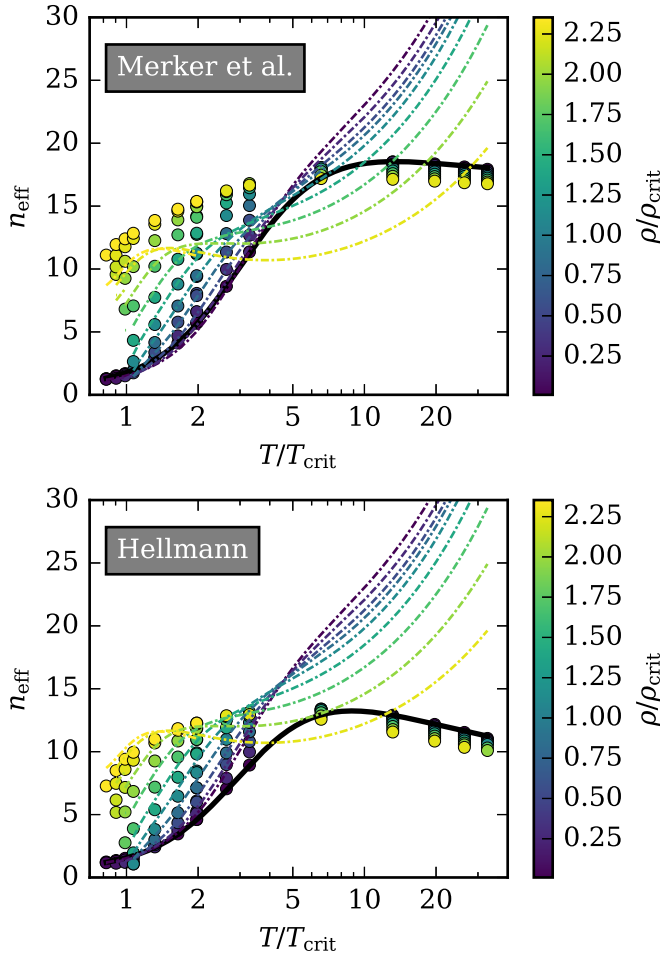


FIG. 13. Results for n_{eff} for CO_2 from the molecular models of Merker *et al.*⁴² and Hellmann⁴⁴. The dashed-dotted curve for each isochore is the same quantity given by the Span and Wagner EOS⁵⁵.

infinite temperature limit go to infinity (see for instance the result for the square-well fluid in Ref. 29).

VI. CONCLUSIONS

Density scaling and entropy scaling can be conceptually aligned by considering density scaling as a mapping onto the residual entropy. The optimal value of n to maximize the correlation between Γ^{-1} and s^+ appears to have some link to the maximum of n_{eff} in the dilute gas limit. For the Lennard-Jones monomer fluid, the maximum is 15.06 (see Fig. 10), and the optimal scaling value is 15.9. For the Lennard-Jones dimer fluid, the maximum value is 18.7 (see Fig. 11), and the optimal scaling value is 17.5. For the Hellman model for CO_2 , the maximum value is 13.24 and the optimal scaling value is 12.1. All scaling values are approximately within one unit of the maximum value. This preliminary observation should be further studied in order to understand whether this relationship should be expected to hold in general. If so, it could offer a route to an entirely predictive approach for entropy scaling

that does not require an equation of state or Monte Carlo methods.

The persistent challenge of both density scaling and entropy scaling is that *a priori* predictions of the functional form of the relationship between the scaled transport properties and the independent variable remain out of reach. The hope is that these observations about the relationship between density scaling and entropy scaling might allow for a new approach bearing more fruit. For instance, it was observed for the Lennard-Jones monomer fluid, and indeed for many other fluids, that there is an approximately exponential relationship between macroscopically scaled viscosity times s^+ to the power of $2/3$ and the residual entropy⁸.

VII. SUPPLEMENTARY MATERIAL

The supplementary material includes a PDF with:

- Figures like Fig. 3, Fig. 4, and Fig. 13 for the other CO_2 models
- Results on change of entropy upon dimerization
- Python snippet for data processing
- Critical region analysis

The complete set of molecular simulation results for CO_2 , Lennard-Jones monomer, and Lennard-Jones dimer models are provided in a zip archive.

ACKNOWLEDGMENTS

Thanks are given to Robert Hellmann for discussion of the relative impact of two- and three-body interactions and Tae-Jun Yoon for discussions of two-body residual entropy. This work was partially supported by the Deutsche Forschungsgemeinschaft (DFG) under grant no. VR 6/16. The simulations were carried out on the Oculus cluster at the University Paderborn and the supercomputer Hawk at the High Performance Computing Center Stuttgart (HLRS) within Project no. MMHBF2. This work was partially supported by the VILLUM Foundation's *MATTER* Grant (No. 16515).

VIII. AUTHOR DECLARATIONS

A. Conflict of Interest

The authors have no conflicts to disclose

B. Data Availability

Data available in article, supplementary material, and linked code repositories. For more detailed information, or additional clarifications, please contact the corresponding author.

- ¹J. C. Dyre, "Perspective: Excess-entropy scaling," *J. Chem. Phys.* **149**, 210901 (2018).
- ²I. H. Bell, "Probing the link between residual entropy and viscosity of molecular fluids and model potentials," *Proc. Natl. Acad. Sci. U.S.A.* **116**, 4070–4079 (2019).
- ³D. Fragiadakis and C. M. Roland, "Connection between dynamics and thermodynamics of liquids on the melting line," *Phys. Rev. E* **83**, 031504 (2011).
- ⁴Y. Rosenfeld, "Relation between the transport coefficients and the internal entropy of simple systems," *Phys. Rev. A* **15**, 2545–2549 (1977).
- ⁵Y. Rosenfeld, "A quasi-universal scaling law for atomic transport in simple fluids," *J. Phys.: Condens. Matter* **11**, 5415–5427 (1999).
- ⁶M. Dzugutov, "A universal scaling law for atomic diffusion in condensed matter," *Nature* **381**, 137–139 (1996).
- ⁷I. H. Bell, R. Hellmann, and A. H. Harvey, "Zero-Density Limit of the Residual Entropy Scaling of Transport Properties," *J. Chem. Eng. Data* **65**, 1038–1050 (2019).
- ⁸I. H. Bell, R. Messerly, M. Thol, L. Costigliola, and J. Dyre, "Modified Entropy Scaling of the Transport Properties of the Lennard-Jones Fluid," *J. Phys. Chem. B* **123**, 6345–6363 (2019).
- ⁹X. Yang, D. Kim, E. F. May, and I. H. Bell, "Entropy Scaling of Thermal Conductivity: Application to Refrigerants and Their Mixtures," *Ind. Eng. Chem. Res.* **60**, 13052–13070 (2021).
- ¹⁰X. Yang, X. Xiao, E. F. May, and I. H. Bell, "Entropy Scaling of Viscosity—III: Application to Refrigerants and Their Mixtures," *J. Chem. Eng. Data* **66**, 1385–1398 (2021).
- ¹¹I. H. Bell, "Entropy scaling of viscosity—II: Predictive scheme for normal alkanes," *J. Chem. Eng. Data* **65**, 5606–5616 (2020).
- ¹²I. H. Bell, "Entropy Scaling of Viscosity – I: A Case Study of Propane," *J. Chem. Eng. Data* **65**, 3203–3215 (2020).
- ¹³R. Casalini and T. C. Ransom, "On the experimental determination of the repulsive component of the potential from high pressure measurements: What is special about twelve?" *J. Chem. Phys.* **151**, 194504 (2019).
- ¹⁴F. Hummel, G. Kresse, J. C. Dyre, and U. R. Pedersen, "Hidden scale invariance of metals," *Phys. Rev. B* **92**, 174116 (2015).
- ¹⁵G. Galliero, C. Boned, and J. Fernández, "Scaling of the viscosity of the Lennard-Jones chain fluid model, argon, and some normal alkanes," *J. Chem. Phys.* **134**, 064505 (2011).
- ¹⁶C. Alba-Simionesco, D. Kivelson, and G. Tarjus, "Temperature, density, and pressure dependence of relaxation times in supercooled liquids," *J. Chem. Phys.* **116**, 5033–5038 (2002), <https://aip.scitation.org/doi/pdf/10.1063/1.1452724>.
- ¹⁷L. Bøhling, T. S. Ingebrigtsen, A. Grzybowski, M. Paluch, J. C. Dyre, and T. B. Schröder, "Scaling of viscous dynamics in simple liquids: theory, simulation and experiment," *New J. Phys.* **14**, 113035 (2012).
- ¹⁸A. Sanz, T. Hecksher, H. W. Hansen, J. C. Dyre, K. Niss, and U. R. Pedersen, "Experimental evidence for a state-point-dependent density-scaling exponent of liquid dynamics," *Phys. Rev. Lett.* **122**, 055501 (2019).
- ¹⁹T. C. Ransom, R. Casalini, D. Fragiadakis, and C. M. Roland, "The complex behavior of the "simplest" liquid: Breakdown of density scaling in tetramethyl tetraphenyl trisiloxane," *J. Chem. Phys.* **151**, 174501 (2019).
- ²⁰J. C. Dyre, "Simple liquids' quasuniversality and the hard-sphere paradigm," *J. Phys.: Condens. Matter* **28**, 323001 (2016).
- ²¹N. Gnan, T. B. Schröder, U. R. Pedersen, N. P. Bailey, and J. C. Dyre, "Pressure-energy correlations in liquids. IV. "Isomorphs" in liquid phase diagrams," *J. Chem. Phys.* **131**, 234504 (2009).
- ²²N. P. Bailey, U. R. Pedersen, N. Gnan, T. B. Schröder, and J. C. Dyre, "Pressure-energy correlations in liquids. I. Results from computer simulations," *J. Chem. Phys.* **129**, 184507 (2008).
- ²³U. R. Pedersen, N. P. Bailey, T. B. Schröder, and J. C. Dyre, "Strong Pressure-Energy Correlations in van der Waals Liquids," *Phys. Rev. Lett.* **100**, 015701 (2008).
- ²⁴T. S. Ingebrigtsen, T. B. Schröder, and J. C. Dyre, "What Is a Simple Liquid?" *Phys. Rev. X* **2**, 011011 (2012).
- ²⁵H. W. Hansen, A. Sanz, K. Adrjanowicz, B. Frick, and K. Niss, "Evidence of a one-dimensional thermodynamic phase diagram for simple glass-formers," *Nature Communications* **9** (2018), 10.1038/s41467-017-02324-3.
- ²⁶ $c_v \equiv T(\partial s/\partial T)_p$, so we may write $c_v^* \equiv T(\partial s^*/\partial T)_p$ or $c_v^*/R \equiv -T(\partial s^*/\partial T)_p$. A similar starting identity of $(\partial s/\partial v)_T = (\partial p/\partial T)_v$ with $v = 1/\rho$ yields the transformation of the numerator.
- ²⁷L. Costigliola, *Isomorph theory and extensions*, Ph.D. thesis, Roskilde University, Denmark (2016).
- ²⁸R. Lustig, "Statistical analogues for fundamental equation of state derivatives," *Mol. Phys.* **110**, 3041–3052 (2012).
- ²⁹I. H. Bell, "Effective hardness of interaction from thermodynamics and viscosity in dilute gases," *J. Chem. Phys.* **152**, 164508 (2020).
- ³⁰T. Maimbourg, J. C. Dyre, and L. Costigliola, "Density scaling of generalized Lennard-Jones fluids in different dimensions," *SciPost Phys.* **9**, 90 (2020).
- ³¹N. Bailey, T. Ingebrigtsen, J. S. Hansen, A. Veldhorst, L. Bøhling, C. Lemarchand, A. Olsen, A. Bacher, L. Costigliola, U. Pedersen, H. Larsen, J. Dyre, and T. Schröder, "RUMD: A general purpose molecular dynamics package optimized to utilize GPU hardware down to a few thousand particles," *SciPost Physics* **3**, 038 (2017).
- ³²S. Deublein, B. Eckl, J. Stoll, S. V. Lishchuk, G. Guevara-Carrion, C. W. Glass, T. Merker, M. Bernreuther, H. Hasse, and J. Vrabec, "ms2: A molecular simulation tool for thermodynamic properties," *Comp. Phys. Comm.* **182**, 2350–2367 (2011).
- ³³C. W. Glass, S. Reiser, G. Rutkai, S. Deublein, A. Köster, G. Guevara-Carrion, A. Wafai, M. Horsch, M. Bernreuther, T. Windmann, H. Hasse, and J. Vrabec, "ms2: A molecular simulation tool for thermodynamic properties, new version release," *Comp. Phys. Comm.* **185**, 3302–3306 (2014).
- ³⁴G. Rutkai, A. Köster, G. Guevara-Carrion, T. Janzen, M. Schappals, C. W. Glass, M. Bernreuther, A. Wafai, S. Stephan, M. Kohns, S. Reiser, S. Deublein, M. Horsch, H. Hasse, and J. Vrabec, "ms2: A molecular simulation tool for thermodynamic properties, release 3.0," *Comp. Phys. Comm.* **221**, 343–351 (2017).
- ³⁵R. Fingerhut, G. Guevara-Carrion, I. Nitzke, D. Saric, J. Marx, K. Langenbach, S. Prokopen, D. Celný, M. Bernreuther, S. Stephan, M. Kohns, H. Hasse, and J. Vrabec, "ms2: A molecular simulation tool for thermodynamic properties, release 4.0," *Comp. Phys. Comm.* **262**, 107860 (2021).
- ³⁶B. Widom, "Some Topics in the Theory of Fluids," *J. Chem. Phys.* **39**, 2808–2812 (1963).
- ³⁷M. S. Green, "Markoff Random Processes and the Statistical Mechanics of Time-Dependent Phenomena. II. Irreversible Processes in Fluids," *J. Chem. Phys.* **22**, 398–413 (1954).
- ³⁸R. Kubo, "Statistical-Mechanical Theory of Irreversible Processes. I. General Theory and Simple Applications to Magnetic and Conduction Problems," *J. Phys. Soc. Japan* **12**, 570–586 (1957).
- ³⁹Z. Zhang and Z. Duan, "An optimized molecular potential for carbon dioxide," *J. Chem. Phys.* **122**, 214507 (2005).
- ⁴⁰J. G. Harris and K. H. Yung, "Carbon dioxide's liquid-vapor coexistence curve and critical properties as predicted by a simple molecular model," *J. Phys. Chem.* **99**, 12021–12024 (1995).
- ⁴¹J. Vrabec, J. Stoll, and H. Hasse, "A set of molecular models for symmetric quadrupolar fluids," *J. Phys. Chem. B* **105**, 12126–12133 (2001).
- ⁴²T. Merker, C. Engin, J. Vrabec, and H. Hasse, "Molecular model for carbon dioxide optimized to vapor-liquid equilibria," *J. Chem. Phys.* **132**, 234512 (2010).
- ⁴³J. Errington, *The Development of Novel Simulation Methodologies and Intermolecular Potential Models for Real Fluids*, Ph.D. thesis, Cornell University (1999).
- ⁴⁴R. Hellmann, "Ab initio potential energy surface for the carbon dioxide molecule pair and thermophysical properties of dilute carbon dioxide gas," *Chem. Phys. Lett.* **613**, 133–138 (2014).
- ⁴⁵P. Mausbach, A. Köster, and J. Vrabec, "Liquid state isomorphism, Rosenfeld-Tarazona temperature scaling, and Riemannian thermodynamic geometry," *Phys. Rev. E* **97**, 052149 (2018).
- ⁴⁶C. S. Murthy, K. Singer, and I. R. McDonald, "Interaction site models for carbon dioxide," *Mol. Phys.* **44**, 135–143 (1981).
- ⁴⁷J. J. Potoff and J. I. Siepmann, "Vapor-liquid equilibria of mixtures containing alkanes, carbon dioxide, and nitrogen," *AIChE Journal* **47**, 1676–1682 (2001).
- ⁴⁸D. Möller and J. Fischer, "Determination of an effective intermolecular potential for carbon dioxide using vapour-liquid phase equilibria from NpT + test particle simulations," *Fluid Phase Equilib.* **100**, 35–61 (1994).
- ⁴⁹J. J. Potoff, J. R. Errington, and A. Z. Panagiotopoulos, "Molecular simulation of phase equilibria for mixtures of polar and non-polar components," *Mol. Phys.* **97**, 1073–1083 (1999).

- ⁵⁰N. Chetty and V. Couling, "Measurement of the electric quadrupole moments of CO₂ and OCS," *Mol. Phys.* **109**, 655–666 (2011).
- ⁵¹R. L. Beil and R. J. Hinde, "Ab initio electrical properties of CO₂: polarizabilities, hyperpolarizabilities, and multipole moments," *Theoretical Chemistry Accounts* **140** (2021), 10.1007/s00214-021-02797-y.
- ⁵²I. Bell, "Archival version of potter," (2022).
- ⁵³I. H. Bell, J. C. Dyre, and T. S. Ingebrigtsen, "Excess-entropy scaling in supercooled binary mixtures," *Nat. Commun.* **11**, 4300 (2020).
- ⁵⁴M. Thol, G. Rutkai, A. Köster, R. Lustig, R. Span, and J. Vrabec, "Equation of State for the Lennard-Jones Fluid," *J. Phys. Chem. Ref. Data* **45**, 023101 (2016).
- ⁵⁵R. Span and W. Wagner, "A New Equation of State for Carbon Dioxide Covering the Fluid Region from the Triple Point Temperature to 1100 K at Pressures up to 800 MPa," *J. Phys. Chem. Ref. Data* **25**, 1509–1596 (1996).
- ⁵⁶E. W. Lemmon, I. H. Bell, M. L. Huber, and M. O. McLinden, "NIST Standard Reference Database 23: Reference Fluid Thermodynamic and Transport Properties-REFPROP, Version 10.0, National Institute of Standards and Technology," <http://www.nist.gov/srd/nist23.cfm> (2018).
- ⁵⁷S. Y. Nezhad and U. K. Deiters, "Estimation of the entropy of fluids with Monte Carlo computer simulation," *Mol. Phys.* **115**, 1074–1085 (2016).
- ⁵⁸B. Scheiner and T. J. Yoon, "Calculation of self-diffusion coefficients in supercritical carbon dioxide using mean force kinetic theory," *J. Chem. Phys.* **154**, 134101 (2021).
- ⁵⁹N. P. Bailey, U. R. Pedersen, N. Gnan, T. B. Schröder, and J. C. Dyre, "Pressure-energy correlations in liquids. II. Analysis and consequences," *J. Chem. Phys.* **129**, 184508 (2008).
- ⁶⁰R. J. Sadus, "Second virial coefficient properties of the n-m Lennard-Jones/Mie potential," *J. Chem. Phys.* **149**, 074504 (2018).
- ⁶¹R. J. Sadus, "Erratum: "Second virial coefficient properties of the n-m Lennard-Jones/Mie potential" [*J. Chem. Phys.* 149, 074504 (2018)]," *J. Chem. Phys.* **150**, 079902 (2019).
- ⁶²S. Polychroniadou, K. D. Antoniadis, M. J. Assael, and I. H. Bell, "A Reference Correlation for the Viscosity of Krypton From Entropy Scaling," *Int. J. Thermophys.* **43** (2021), 10.1007/s10765-021-02927-5.